CAMP ROCK FAULT SLIP RATE AND FOLDING OF THE LENWOOD ANTICLINE: CONTRIBUTIONS TO EASTERN CALIFORNIA SHEAR ZONE STRAIN ACCUMULATION

Emily Gurney

A thesis submitted to the faculty of the University of North Carolina at Chapel Hill in partial fulfillment of the requirements for the degree of Master of Science in the Department of Geological Sciences

Chapel Hill
2008

Approved by:
Dr. Mike Oskin
Dr. Kevin Stewart
Dr. Allen Glazner

ABSTRACT

EMILY GURNEY

Camp Rock fault slip rate and folding of the Lenwood anticline: contributions to eastern California shear zone strain accumulation
(Under the direction of Dr. Mike Oskin)

Geologic mapping, ^{10}Be geochronology, and fold modeling provide insight into reconciling discrepant geologic and geodetic slip rates across a portion of the eastern California shear zone. The Camp Rock fault is one of six faults that make up the shear zone. Two alluvial fans of different generations, offset by the fault, yield ages of 100±30 ka and 56.4±7.7 ka. Offsets on these fans are 41±25 m and 22±2 m respectively, yielding a long-term slip rate of 0.4 +0.3/-0.1 mm/yr for the fault. This is only 2-7% of the geodetic strain rate across the shear zone. The Camp Rock fault terminates northward into the Lenwood anticline. Modeling of this fold indicates ~3.8 km of north-south shortening, of which ~1.0-2.4 km is not transferred to Camp Rock fault slip but is maintained east of the fault. Such regionally distributed shortening may help to reconcile geologic and geodetic strain rates.

ACKNOWLEDGMENTS

I would like to thank my advisor Mike Oskin for his guidance on this project and his patience for its completion, as well as my committee members Kevin Stewart and Allen Glazner for their reviews and advice on various portions of this thesis. I am especially grateful to Stefanie Bernosky for her assistance in the field as well as to the other geomorphology students at the University of North Carolina: Kim Le, Michael Strane, Eitan Shelef, Sabrina Belknap, Jacob Selander and Scott Bennett for answering all of my questions, large or small. Without the assistance of Dylan Blummentritt at the University of Minnesota and use of the cosmogenic laboratory there, I would not have been able to finish this project. Lastly I would like to thank my parents for their moral support during completion of my thesis.

TABLE OF CONTENTS

LIST OF TABLES

LIST OF FIGURES

INTRODUCTION

The eastern California shear zone (ECSZ) provides a natural laboratory in which to study tectonic strain accumulation and its release as fault slip. It is an example of a distributed, intracontinental shear zone with a long geodetic record and well-documented paleoseismicity (Sauber et al., 1986; Dawson et al., 2003). These data indicate a potential discrepancy between faster geodetic and slower geologic strain rates. Long-term (10^5 yr) fault slip rates can test if high geodetic strain rates or low rates of paleoseismicity are more representative of the long-term behavior of the faults of the ECSZ (e.g. Oskin and Iriondo, 2004).

The Mojave Desert portion of the ECSZ refers to a block bounded to the north by the sinistral Garlock fault, to the southwest by the dextral San Andreas fault, and to the east by the southern extension of the Death Valley fault zone (Glazner et al., 2002; Figure 1). This portion of the ECSZ lies to the northeast of the Big Bend segment of the San Andreas fault where shortening has built the Transverse Ranges (Crowell, 1981). This study focuses on the Camp Rock fault, which is located in the central Mojave Desert, and lies within an array of six dextral faults that comprise the ECSZ south and east of Barstow, California. From west to east, these faults are the Helendale, Lenwood, Camp Rock, Calico, Pisgah and Ludlow (Figure 2).

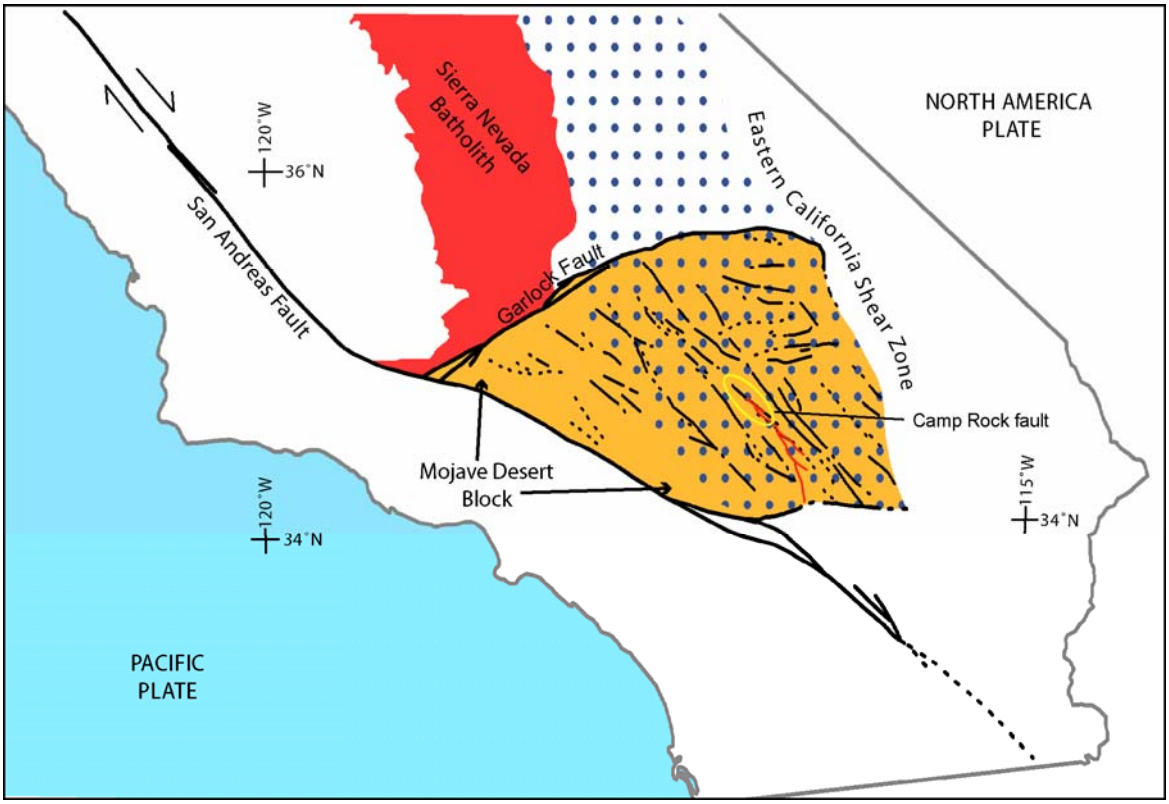

Figure 1: Index map of Pacific-North America plate boundary through southern California. Major faults are shown as thick black lines; thinner black lines represent faults of the Mojave Desert portion of the eastern California shear zone. Faults highlighted in red indicate extent of 1992 Landers Earthquake rupture, which includes the southern portion of the Camp Rock fault (Sieh et al., 1993). Orange area is Mojave Desert block, red area is Sierra Nevada batholith, blue dots show extent of the eastern California shear zone.

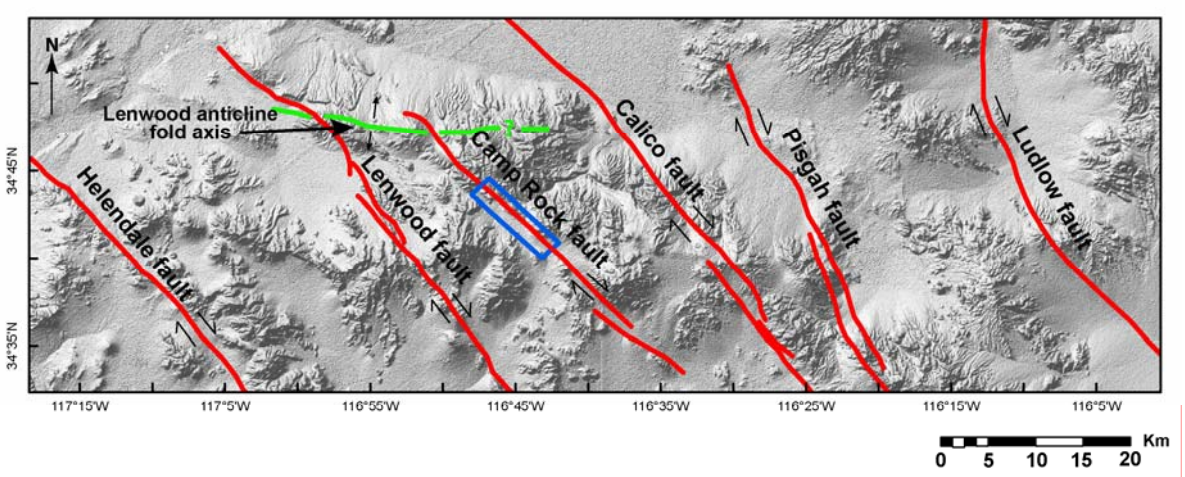

Figure 2: Index map showing the six faults of the central Mojave Desert portion of the eastern California shear zone. Background is hillshaded with a 30m-pixel elevation model. Faults are represented by red lines. Green line indicates trace of Lenwood anticline fold axis. Blue box shows location of LiDAR swath.

Objective

This thesis presents a slip rate for the Camp Rock fault and a shortening estimate for the Lenwood anticline, into which the northern Camp Rock fault terminates (Figure 2). Data collected on the Camp Rock fault and Lenwood anticline will contribute to assessment of the total long-term rate of dextral faulting of the ECSZ. The Camp Rock fault is of particular interest because of its intersection with the actively folding Lenwood anticline to the northwest and because of existing paleoseismic data (Rubin and Sieh, 1997). This study analyzes both faulting and folding together to provide insight into interactions between faults and shortening structures in the Mojave Desert portion of the ECSZ.

Tectonic History

Dibblee (1961) first proposed that NW-trending dextral faults of the ECSZ are related to movement along the San Andreas fault. Earlier, Hewett (1954) had proposed that these faults exhibited mainly dip-slip motion. Atwater (1970) noted that motion on faults of the Mojave Desert portion of the ECSZ was most likely accommodating a portion of Pacific - North America plate boundary motion, thus accounting for a discrepancy between San Andreas fault slip rate and Pacific-North America plate motion rate. Recent measurements of Pacific-North American plate motion in southern California are ~50 mm/yr (DeMets and Dixon, 1999) and measurements of San Andreas fault motion are ~35 mm/yr (Sieh and Jahns, 1984). Based on reconstruction of a block model, Dokka and Travis (1990) argue that faults of the Mojave Desert portion of the ECSZ accommodate approximately 9-14% of relative motion between the Pacific and North American plates, or 4.5-7 mm/yr. Geodetic measurements of displacement across

the ECSZ are about twice this, or 10-14 mm/yr (Savage et al., 1990; Dixon et al., 1995; Gan et al., 2000; Miller et al., 2001). This higher rate accounts for most of the difference between the displacement rate across the Pacific-North American plate boundary, and the slip rate of the San Andreas fault in central California (Miller et al., 2001). Tectonic models of the Mojave ECSZ emphasize the role of dextral shear. Early models of the Mojave Block by Garfunkel (1974) and Carter et al. (1987) treated the entire area as a zone of distributed simple shear during the late Cenozoic. Dokka and Travis (1990) later designated the zone of regional dextral shear defined by the Mojave Desert block and dextral faulting north of the Garlock fault as the eastern California shear zone. They divided the Mojave Desert block into a series of strain domains that have deformed and rotated independently of one another.

The timing of initiation of the ECSZ is uncertain. Dokka and Travis (1990) hypothesize that initiation of motion along dextral faults of the ECSZ likely occurred due to Pacific – North American plate boundary interaction causing broadly distributed regional dextral shear. They place the time of initiation at 6-10 Ma based on earlier work of Carter et al. (1987) and Stewart (1983). Carter et al. (1987) documented that shearing younger than 10 Ma caused rotation of the Eastern Transverse Ranges and Stewart (1983) found that faulting may have begun as late as 6 Ma by establishing age relations on northwest-striking dextral faults in Death Valley. Glazner et al. (2002) further this idea with the hypothesis that northward migration of the Mendocino triple junction away from the Mojave Desert region is related to the change from an extensional to a transpressional deformation regime. However, this would place the onset of dextral shear at 19 Ma

(Glazner et al., 2002), significantly earlier than the ages argued by Dokka and Travis (1990).

Disagreements over the timing of fault inception are accompanied by differing ideas over the roles of shortening and extension in the central Mojave Desert. It is agreed upon that extension commenced in the Mojave Desert during the latest Oligocene or earliest Miocene (Dokka, 1983; Bartley et al., 1990; Glazner et al., 2002). However, these authors disagree on the spatial and temporal scope of extension. Bartley et al. (1990), Fletcher et al. (1995) and Glazner et al. (2002) show that extension by detachment faulting in the latest Oligocene was intense to the immediate west and northwest of Barstow, resulting in exhumation of a metamorphic core complex, but was minimal or nonexistent outside of that area. Dokka (1989) hypothesizes that extension in the earliest Miocene was intense in the western and central Mojave Desert, and proposes that this extensional tectonism was concentrated in the east-west trending Mojave Extensional Belt.

Bartley et al. (1990) and Glazner et al. (2002) maintain that dextral faulting in the central and western Mojave Desert began immediately after regional extension terminated, and that regionally significant north-south contraction accompanies strike-slip faulting and may equally participate in accommodating strain in the Mojave Desert. Their observation that possible Quaternary age deposits are folded indicates that contraction is likely still continuing at the present time (Bartley et al., 1990). This differs greatly from the view of Dokka and Travis (1990), who maintain that on a regional level, strike-slip faulting has been coeval with extension in the Mojave Desert since the late Miocene, and extension has been overprinted by dextral shear. The authors state that

areas of shortening are local, minor components of the total strain accumulation in the ECSZ and are limited to the northernmost tips of dextral faults in response to rotation of the Mojave Desert block.

Discrepancies Between Geologic and Geodetic Data

Potential discrepancies exist between geologic fault slip rates and geodetic strain accumulation rates across the Mojave Desert portion of the ECSZ. Estimates of present-day geodetic strain accumulation rate across the area range from 10 to 14 mm/yr (Savage et al., 1990; Dixon et al. 1995; Gan et al. 2000; Miller et al. 2001). Sauber et al. (1994) show that distribution of strain across this portion of the ECSZ (~12 mm/yr) extends at least from the Helendale fault (westernmost active fault in the Mojave Desert ECSZ) to the Pisgah fault, a zone 60 km wide. Paleoseismic investigations, however, do not support this high geodetic strain accumulation rate. Rockwell et al. (2000) found that earthquakes on distinct faults of the ECSZ, including the southern Camp Rock fault, are temporally clustered with a return period of at least ~5000 years. The most recent cluster of earthquakes includes the 1992 Landers earthquake and the 1999 Hector Mine earthquake. Assuming an average slip-per-event similar to the ~3m documented for the 1992 and 1999 earthquakes (Sieh et al., 1993; Treiman et al., 2002), the paleoseismic data implies that earthquake production rates and thus slip rates for faults in the eastern California shear zone are uniformly low: approximately 0.6 mm/yr per fault, or approximately 4 mm/yr across the entire shear zone.

Paleoseismicity of the Emerson fault, an en echelon southward continuation of the Camp Rock fault, is consistent with the data of Rockwell et al. (2000). Rubin and Sieh (1997) found that earthquakes recur infrequently on the Emerson fault –

approximately every 9 kyr. Based on the paleoseismic data and an assumed displacement of 6 meters per earthquake (maximum observed surface displacement for the 1992 Landers earthquake), these authors calculated a maximum slip rate on the Emerson fault of ~0.7 mm/yr, only one-fourteenth to one-twentieth of the geodetic strain rate across the entire Mojave Desert portion of the ECSZ. A minimum calculated slip rate of 0.2 mm/yr contributes one-fiftieth, at most, to the overall geodetic strain rate. This result indicates that the Emerson fault and likely also the Camp Rock fault contribute little to overall strain accumulation in the ECSZ (Rubin and Sieh, 1997). However, if the clustering hypothesis of Rockwell et al. (2000) is correct, and all faults produce similar, infrequent earthquakes, then these rates could be representative of the shear zone overall.

New kinematic models for the ECSZ created by McQuarrie and Wernicke (2005) suggest a long-term sum slip rate of 8.3±1 mm/yr, significantly lower than geodetic rates of 10-14 mm/yr. They propose that shear began at ~16 Ma and reached its current long-term rate by 12 Ma. Higher offsets on individual faults of the central Mojave Desert were required for kinematic compatibility with the ECSZ north of the Garlock fault. For example, they predict 11-13 km of slip for the Camp Rock fault, whereas geologic markers mapped by Dibblee (1964) are only offset 2-4 km according to studies by Hawkins (1976) and Miller (1980; Figure 3). Regional penetrative shear within the granitic crust between strike-slip faults may account for the differences between model and observed data; however, it is unclear which structures are accommodating this shear (McQuarrie and Wernicke, 2005). The presence of contractional features such as ubiquitous active folds found in the central Mojave Desert could be one mechanism accommodating additional shear, and could reconcile geologic slip rates and geodetic

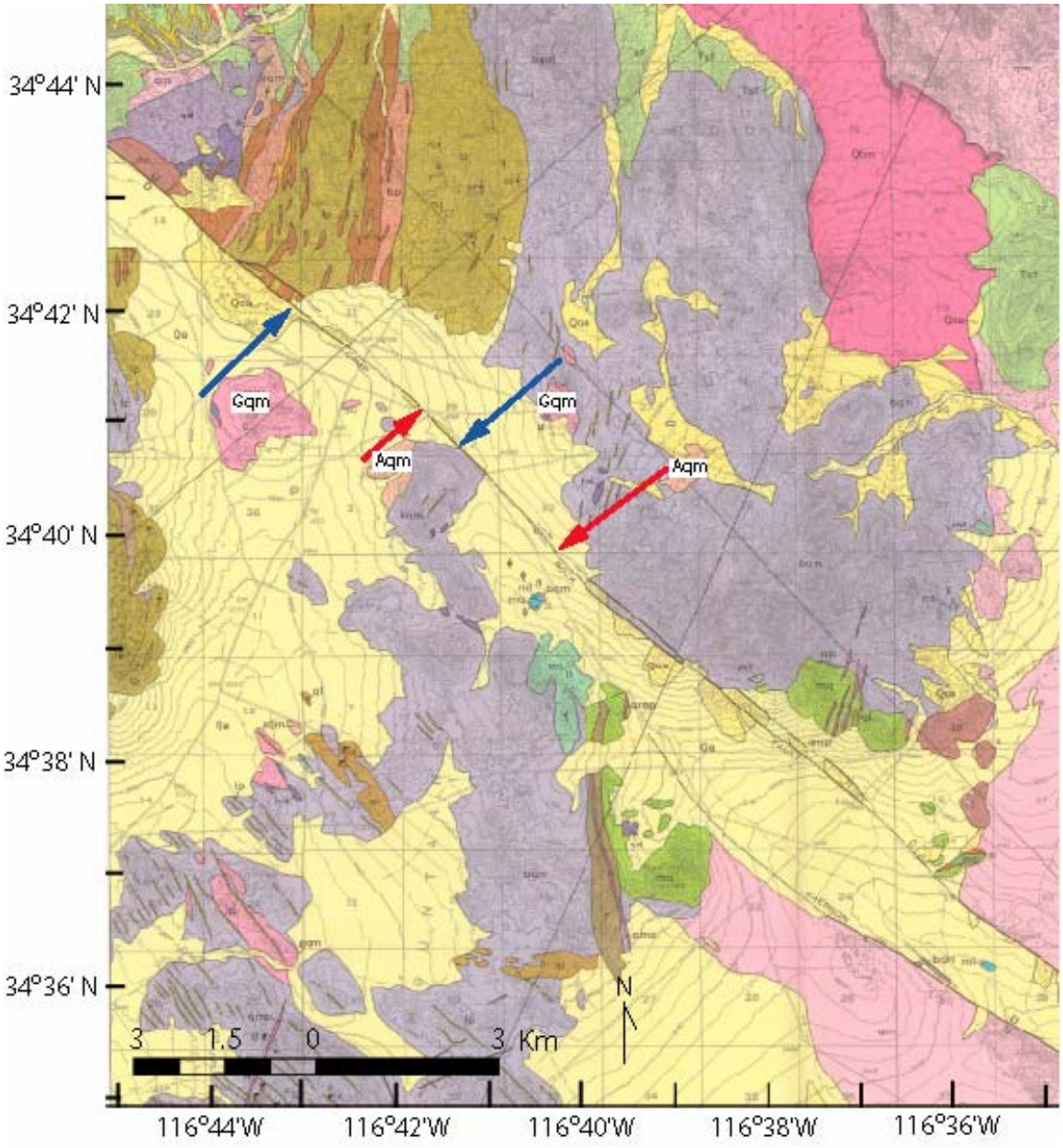
34°44' N
34°42' N
34°40' N
34°38' N
34°36' N
Gqm
Gqm
Aqm
Aqm
N
3 1.5 0 3 Km
116°44'W
116°42'W
116°40'W
116°38'W
116°36'W

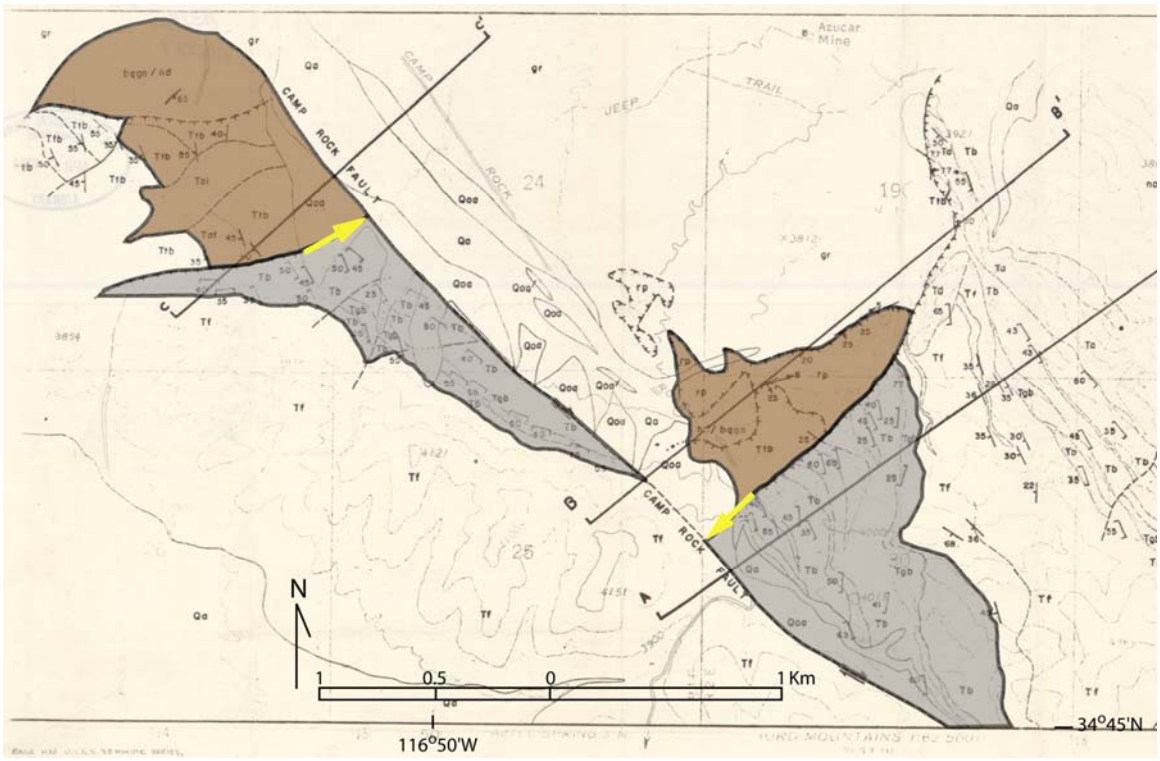

Figure 3. Total offset measurements of the Camp Rock fault. Top figure shows an offset series of small outcrops including granite and quartz monzonite (Gqm; blue arrows) and aplitic quartz monzonite (Aqm; red arrows). Base map by Dibblee, 1964. 3.75 km of offset between the units is from Miller, 1980. Bottom figure shows a 2 km offset of a non-depositional contact between interbedded volcanic and sedimentary rocks (gray shaded area) and steeply dipping tuff breccia overlying gneiss and hornblende diorite and biotite granite (brown shaded area). Map area is located just southeast of the core of the Lenwood anticline. Yellow arrows indicate location of contact. Map modified from Hawkins, 1976.

strain rates (Bartley et al., 1990).

Study Area

This study focuses on the northern portion of the Camp Rock fault, bounding the west side of the Newberry and Rodman Mountains, and the Lenwood anticline, into which the Camp Rock fault terminates. This area was selected for a slip rate study because the fault trace cuts through many alluvial fan surfaces, thereby increasing the likelihood of locating measurable and dateable offsets. The study area also contains alluvial fan surfaces composed of unique clast types which aids correlation of alluvial fans for offset measurement. The Lenwood anticline is an active east-west trending fold located at the northwest end of the Camp Rock fault (figure 2). As the Camp Rock fault approaches the fold, its strike changes from 325° to 290°, and fault slip diminishes from 2-4 km to zero.

METHODS

Mapping

Two separate maps were created, one along the Camp Rock fault and another across the Lenwood anticline. Plate 1 is a detailed map of Quaternary units and bedrock along the Camp Rock fault. Pre-Quaternary stratigraphic units are adapted from mapping by Dibblee (1964). The map also segregates various generations of Quaternary deposits in order to locate features with measurable fault displacement. Airborne Laser Swath Mapping via LiDAR (light detection and ranging) was acquired as a mapping base for its high resolution and precise elevation data. LiDAR was processed to 1 m pixels and is accurate to 0.1 m in the vertical. This makes it extremely useful for mapping fault scarps in active alluvium and other Quaternary surfaces where the scarps may be difficult to discern in the field. The high resolution provides ease of locating single-event fault scarps and is helpful in targeting features before field work commences. Maps produced in the field at a scale of 1:5,000 were later digitized using ArcGIS software, providing a continuous map of a 10-km section the Camp Rock fault. Figure 4 is a strip map across the axis of the Lenwood anticline. This map is based on mapping by Dibblee (1970) and modified from field measurements compiled on aerial photos at a scale of 1:10,000. Mapping of the Lenwood anticline was subsequently used to create a cross-section of the fold.

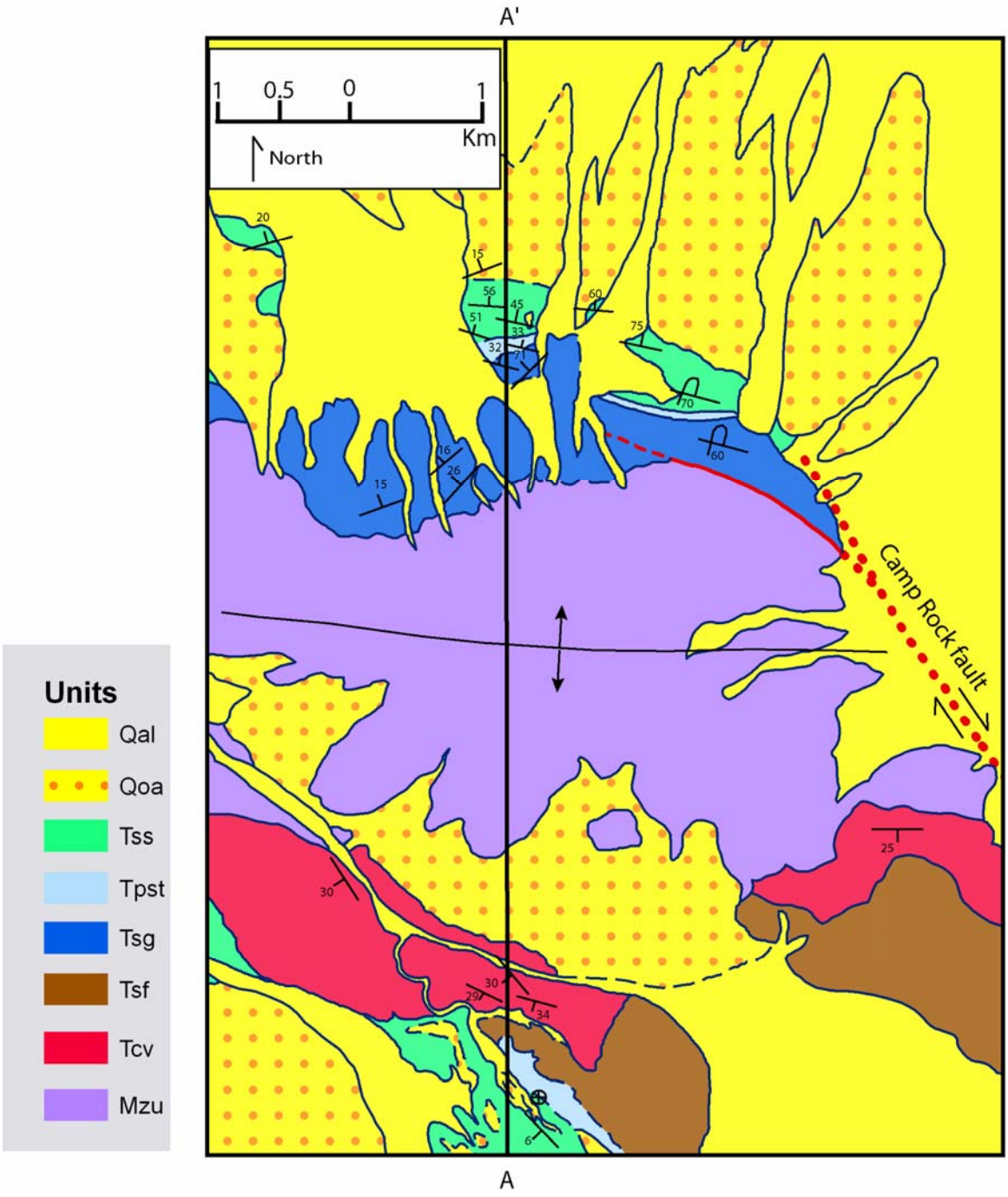

Figure 4. Geologic map of a portion of the Lenwood anticline. Line A-A' indicates location of cross-section. Map modified from Dibblee (1970).

^{10}Be Geochronology

Along with detailed Quaternary mapping and location of an offset alluvial fan surface along the Camp Rock fault, cosmogenic dating, using in-situ accumulation of ^{10}Be in quartz, was performed to determine an age for the offset fan surface. Clasts were collected from darkly varnished pavements on the fan surface in three locations. Two samples were also taken from modern alluvium in order to estimate ^{10}Be concentration inherited prior to deposition of the sediment onto the fan surface. Sample preparation took place according to the standard operating procedures of the cosmogenic dating lab at the University of Minnesota – Minneapolis, under the direction of Dr. Lesley Perg. Sample preparation methods are described in Appendix A. ^{10}Be measurements took place at the Lawrence Livermore National Laboratory.

RESULTS AND INTERPRETATIONS

Stratigraphy

Mesozoic basement rocks are prevalent east of the Camp Rock fault in the Rodman Mountains and along both sides of the fault in the Newberry Mountains, as well as in the core of the Lenwood anticline. Miocene sedimentary and volcanic rocks of the Pickhandle Formation are present in the Newberry Mountains. The Pickhandle Formation and Miocene sedimentary rocks of the Barstow Formation are present on the limbs of the Lenwood anticline, overlying the basement rock unconformably. Modern alluvium and older alluvial fans are present both along the Camp Rock fault and on the limbs of the Lenwood anticline.

Mesozoic Basement Rocks

Porphyry Complex (Mzpc)

The porphyry complex consists of massive, hard, mostly dark-gray fine-grained porphyritic metavolcanic rocks. Some members of the complex range from light-gray to pink and white. Phenocrysts of plagioclase, quartz and potassium feldspar are common (Dibblee, 1964). Internal units of the complex were not differentiated during mapping. Outcrops are present in the Rodman Mountains adjacent to the Camp Rock fault, in the southern part of the study area.

Quartz Diorite (Mzqd)

The quartz diorite is light-gray to gray, massive, equigranular and medium-grained. It is composed mainly of quartz, plagioclase, potassium feldspar and biotite. Outcrops are present on the border of the Rodman and Newberry Mountains adjacent to the Camp Rock Fault and west of the Camp Rock fault in the northern part of the study area.

Undifferentiated basement rocks (Mzu)

Mesozoic basement units were not differentiated during mapping of the Lenwood anticline. Dibblee (1970) mapped granite, hornblende diorite and gabbro, biotite quartz monzonite, aplitic quartz monzonite, and an andesite to latite porphyry exposed in the core of the Lenwood anticline.

Miocene Sedimentary and Volcanic Rocks

Mixed-clast Conglomerate (Tsf)

The mixed-clast conglomerate is gray to brown and unconsolidated. Clasts are unsorted, subrounded to angular boulders, cobbles and pebbles derived from the porphyry complex, quartz diorite, and other plutonic rocks not found within the mapping area. The conglomerate also contains clasts of basalt and andesite (Dibblee, 1970). Bedding is not exposed. It is interpreted to have been deposited as alluvial fans, presumably derived from areas to the south (Dibblee, 1970). The unit is located along both sides of the Camp Rock fault in the Newberry and Rodman Mountains, as well as on the south limb of the Lenwood anticline.

Quartz Diorite Conglomerate (Tcgqd)

The quartz diorite conglomerate is a gray and unconsolidated monolithologic conglomerate of subangular to angular boulders, cobbles and pebbles. The unit is derived from quartz diorite exposures adjacent to the Camp Rock fault. In places, the conglomerate was shed across the fault and sits atop quartz diorite unconformably. The quartz diorite conglomerate appears to have been deposited along the Camp Rock fault scarp, and is likely derived from erosion of the scarp. Based on the angularity of clasts and its presumed connection to Camp Rock fault activity, the quartz diorite conglomerate could possibly be younger than Miocene in age. It is found locally on two hills in the northwestern Rodman Mountains west of and within the Camp Rock fault zone.

Undifferentiated volcanic rocks and conglomerate (Tcv)

Undifferentiated volcanic rocks and conglomerate consist of agglomerate, a tuff breccia, a granitic breccia and a basalt unit. The agglomerate and tuff breccia is white to tan and consists of mainly unsorted porphyritic rhyolite clasts. The basalt is black and massive and is microcrystalline to fine grained. The granitic breccia is shattered biotite quartz monzonite in landslide masses or gray granitic breccia (Dibblee, 1970). Outcrops are present on the south limb of the Lenwood anticline.

Granitic conglomerate (Tsg)

The granitic conglomerate is white-pink to light gray. Clasts range in size from <1 cm to boulder-sized in a sandstone matrix (Dibblee, 1970). Bedding is rare. It directly overlies eroded pre-Tertiary volcanic rocks. Outcrops are present on the north and south limbs of the Lenwood anticline, but it is found predominantly on the north limb.

Peach Springs Tuff (Tpst)

The Peach Springs Tuff is a white to pink nonlithified to lithified tuff. It contains subrounded to angular potassium feldspar phenocrysts up to 2 mm in diameter, small xenoliths of pink and brown volcanic rocks, and biotite (Dibblee, 1970). It crops out on the north and south limbs of the Lenwood anticline, with outcrops on the south limb more friable than those on the north.

Sandstone/shale/conglomerate (Tss)

The sandstone is white to light gray-tan with localized orange-pink to tan areas. It weathers brown. Grains are subangular to subrounded and poorly sorted. The outcrops are mostly massive with some shaley bedding found in the outcrops on the north limb of the Lenwood anticline. The shale unit is micaceous and includes interbedded gray to tan shale and sandstone (Dibblee, 1970). The conglomerate clasts are rounded to subangular and composed of Tertiary andesites and Mesozoic granites. Outcrops are present on the north and south limbs of the Lenwood anticline.

Quaternary Units

Five distinct Quaternary units are distinguished adjacent to the Camp Rock fault. Only modern alluvium and undifferentiated old alluvium (*Qoa*) are distinguished on the limbs of the Lenwood anticline.

Older alluvium along the Camp Rock fault has been subdivided into three alluvial fan generations, *Qtf*, *Qtk* and *Qtn*. In this naming scheme, *Q* refers to the Quaternary age of the fans, *t* indicates that they are terraces, and *f, k* and *n* are letters chosen at random to indicate the relative age of each terrace generation, where letters closer to the beginning of the alphabet represent older alluvial fans. Letters successively lower in the alphabet

represent successively younger fans. Pre-existing naming schemes were not used, in order to remove any association of the age of these fans with past glacial or interglacial periods.

All three generations are located adjacent to the fault, in the form of terraces that sit higher than the modern alluvium or against the mountain front. These alluvial fans, formed by channels emerging from mountains adjacent to the Camp Rock fault, are important geomorphic features for measuring fault offset. Abandonment of alluvial fans, forming relict surfaces, occurs via a transition from aggradation of channel-transported alluvium to channel incision. The former aggradational surface becomes abandoned and soil development processes commence. This cycle can result in multiple generations of surfaces preserved in order of formation, with younger surfaces inset successively below older surfaces. Elsewhere, younger surfaces grade to fans deposited above older deposits, obscuring older fan surfaces.

Alluvial fan generations were distinguished based on relative age criteria. In addition to inset relations between fans, the presence or absence and intensity of rock varnish and rubification of clasts, and the extensiveness of desert pavement on the fan surface were used as diagnostic tools. Rock varnish is a brownish-black manganese-rich coating that accumulates on top of clasts that are resting on a stable surface in an arid region (Bull, 1991). The bottom sides of these clasts undergo rubification, which is the accumulation of an orange to reddish-brown coating of iron-rich rock varnish (Bull, 1991). Older fans will have clasts that have undergone a higher degree of varnishing and rubification than younger fans. Development of desert pavement also increases with age of surface. A pavement is formed as aeolian processes winnow away

small particles on a fan surface, allowing larger and more similar-sized clasts to become packed in against one another in an interlocking arrangement. An accretionary Av soil horizon of aeolian dust that becomes entrapped below the pavement helps to keep the pavement clasts at the surface (Wells et al., 1995) and facilitates surface smoothing through shrink-swell processes. Well-developed pavements will have a smooth surface, typically comprised of well-varnished clasts, whereas younger surfaces with no pavement will have a topographically variegated surface consisting of bars and swales. The amount of vegetation present on the surface can also be used in relative dating, as younger surfaces are more conducive to plant growth than older surfaces.

Qtf alluvial fans (Qtf)

Qtf is the oldest fan generation. It displays a high degree of dark brown to black desert varnish, and dark orange to red rubification on all clasts. The presence of well-interlocked, continuous desert pavement creates a smooth surface and allows for almost no gaps between clasts (Figure 5). Bar and swale topography is completely obliterated. Terrace surfaces are almost completely devoid of vegetation. Large clasts are scattered in small clusters across the surface. Based on clast composition, some *Qtf* fans can be tied to local alluvial sources that have subsequently been displaced by fault slip.

Qtk alluvial fans (Qtk)

Qtk fans are younger than *Qtf* fans based on inset relations and morphology. Some clasts display brown to black desert varnish. However, many clasts are unvarnished to only lightly varnished. Rubification is less developed than on *Qtf* surfaces and is orange when present. Poorly interlocked desert pavement is patchy and sand- to gravel-sized particles are found between larger clasts (Figure 6). The fans exhibit

subdued bar and swale topography and few plants grow on their surfaces. Large clasts appear scattered throughout, but are found in larger quantities on remnant channel bars.

Qtn alluvial fans (Qtn)

Qtn is the youngest fan generation based on inset relations and morphology. Surfaces are light in color as they display the most minimal desert varnish or none at all. Rubification is light orange if present. Desert pavement is nonexistent and large clasts lie loosely on the surface. Bar and swale topography is preserved and plants grow abundantly on the surface. The largest clasts are located atop the remnant bar crests (Figure 7).

Modern alluvium (Qal)

Two types of modern alluvium exist: inactive alluvial fans and active washes. However, the two types were not differentiated during mapping. The inactive alluvial fans are located to the southwest of the fault and emanate from the mountain front. They contain gravel, cobbles and large amounts of sand and display very well-preserved bar and swale topography. The active washes are located in the valley to the southwest of the fault. They are also composed of sand, gravel and cobbles but contain more gravel than the inactive alluvial fans. Bar and swale topography in active alluvium can reach up to approximately a meter high.

Silt (Qsi)

Silts of lacustrine or aeolian origin are present along the southwest side of the fault underlying thin terrace gravel deposits. The silt is white to light brown in color, unconsolidated, and contains calcite cementation in some areas.

Figure 5: *Qtf* terrace surface. The black clasts display a high degree of varnish, and the undersides of these same clasts are orange-red due to rubification. Visible rubification of clasts is due to overturning of clasts. The tightly packed angular clasts indicate a well-developed desert pavement, with few smaller clasts present between the larger interlocked clasts.

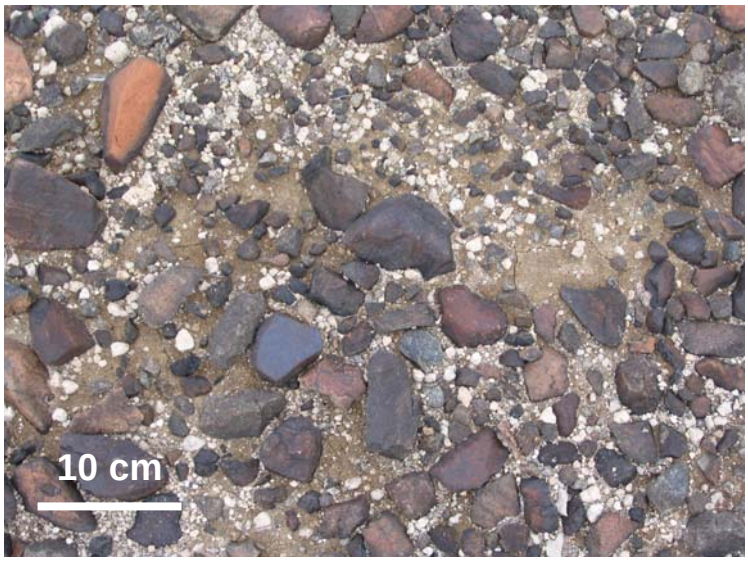

Figure 6: *Qtk* terrace surface. Note that although some clasts display black or brown desert varnish, smaller clasts are commonly unvarnished. Rubification is less common and a lighter orange when present. Poorly interlocked clasts constitute a patchy desert pavement that contains sand- to gravel-sized particles between larger clasts.

Figure 7: *Qtn* terrace surface. Desert varnish is minimal if at all present, and rubification of the lightest orange is rarely present. Desert pavement is nonexistent, as a wide spectrum of clast sizes lie loosely on the surface.

Colluvium (Qc)

Colluvium consists of pebble- to boulder-sized angular to subangular clasts of various composition in a coarse sand matrix. The colluvium forms aprons covering parts of the Camp Rock fault scarp.

Mapping of Camp Rock Fault

I subdivide mapping of the northern Camp Rock fault into four divisions with distinct attributes. The southern section comprises the southern 3.3 km of the fault trace and the surrounding area, the mid-southern section the next 1.9 km, the mid-northern section the following 3.3 km, and the northern section encompasses the northern 2.3 km.

In the southern section, the fault is characterized by a single, distinct trace which is at times apparent as a fresh scarp or a scarp visible in modern alluvium from the 1992 Landers earthquake. Basement rocks located in the Rodman Mountains east of the fault are comprised of several members of the porphyry complex. An expansive alluvial fan complex emanates from the mountain front, dominated by *Qtf* and *Qtk* alluvial fans. The *Qtf* portion of this fan is cut by channels up to ~5 m deep.

The Camp Rock fault throughout the mid-southern section is predominantly covered by modern alluvium as its trace runs along the range front. Only for a few meters at a stretch is its trace clearly located by an apron of colluvium or as the contact between Miocene rocks and small *Qtn* terrace remnants. The Mesozoic rocks located east of the fault are composed of the porphyry complex and quartz diorite. The contact between these basement rocks is covered by the Miocene mixed-clast conglomerate. Modern alluvium makes up almost the entire southern side of the fault throughout this section, with the exception of two small *Qtf* alluvial fan remnants.

The geology of the mid-northern section is significantly more complex than the preceding two sections. The main strand of the fault twice splays into two segments as it runs through hills of Mesozoic quartz diorite covered by Miocene conglomerate, in the Rodman Mountains. Quartz diorite conglomerate emplaced coevally with fault slip overlies quartz diorite bedrock on two hills south of the fault. Although the fault in this section cuts through bedrock, the southern side of the fault is predominantly alluvium and old alluvial surfaces. A thrust fault strand cuts Quaternary alluvium on the south side of the main fault. At the mountain front, terraces of all three generations exist, although the prevailing generation is *Qtk*. Many of the terraces in this area are thin deposits overlying silt.

In the northern section the fault runs along the side of an elongate ridge before splitting into two branches. The fault is more difficult to precisely locate in this section due to a paucity of offsets of topographic features. Miocene conglomerate (*Tsf*) of the Newberry Mountains occurs on both sides of the fault. Little modern alluvium exists in this section. Fan surfaces of all three generations are present but scarce.

Evidence of paleoquakes along the Camp Rock fault is present in the form of fault scarps. Fault scarps in terraces have the general appearance of either a small step or a groove in the fan surface. These scarps are commonly very small, only a few centimeters in height, and are oftentimes better viewed in the LiDAR than in the field. More prominent scarps exist as slope breaks on hillsides or steps in fans up to 1 m in height, although scarps of this magnitude are less common. Toward the southern end of the study area, fresh scarps from the northernmost rupture of the 1992 Landers earthquake are observed (Plate1).

^{10}Be Geochronology Results

Ages of the five collected samples were calculated using the equation

$$t=N/P_0,$$

where N is the concentration of ^{10}Be atoms/quartz gram of the sample, P_0 is the production rate of ^{10}Be atoms at the surface, and t is exposure time of the sample (Lal, 1991). This equation assumes that decay of ^{10}Be, with a half-life of 1.36 Ma, is negligible. A P_0 of 11.1 (atoms/gram)/year was calculated based on an altitude of 1147 m and a latitude of ~34^{o} N (Stone, 2000). Of the five samples collected along the Camp Rock fault, samples CR-01, CR-02 and CR-03 were collected from the *Qtf* fan surface and samples CR-04 and CR-06-01 were collected from the modern alluvium. The concentrations found for the modern alluvium represent inheritance of ^{10}Be during erosion and transport of sediment prior to deposition on the alluvial fan to be dated (Anderson et al., 1996). This concentration is used to estimate and subtract inheritance from the concentrations of the alluvial fan samples. Calculated exposure times have been rounded to the nearest 1 ka and include 1σ errors.

Table 1: ^{10}Be concentrations and exposure ages

Sample	^{10}Be concentration $\times 10^5$ (atoms/g quartz)	Inheritance-corrected ^{10}Be concentration $\times 10^5$ (atoms/g quartz) using sample CR-06-01	Inheritance-corrected ^{10}Be concentration $\times 10^5$ (atoms/g quartz) using weighted mean of CR-04 and CR-06-01	Inheritance-corrected exposure time using sample CR-06-01 (ka)	Inheritance-corrected exposure time using weighted mean of CR-04 and CR-06-01 (ka)
CR-01	18.2±0.6	12.0±1.6	11.4±1.1	108±15	103±11
CR-02	14.7±0.18	8.7±1.5	7.9±0.96	78±14	71±9
CR-03	8.77±0.17	2.8±1.5	1.97±0.96	25±13	18±8
CR-04	8.14±0.11	—	—	—	—
CR-06-01	5.99±1.5	—	—	—	—
Weighted mean CR-04 and CR-06-01	6.8±0.94	—	—	—	—

Age of *Qtf* Fans

The samples from the *Qtf* surface yield inheritance-corrected exposure ages of 108±15 ka, 78±14 ka and 25±13 ka using the ^{10}Be concentration of CR-06-01, and 103±11 ka, 71±9 ka and 18±8 ka using the ^{10}Be concentration of the weighted mean of CR-04 and CR-06-01. The youngest age, from sample CR-03, is stratigraphically inconsistent with ages of the younger *Qtk* surface determined along the nearby Calico fault (Oskin et al., 2007). The anomalously young CR-03 age probably indicates erosion on the fan surface at the sample site. Of the two samples from the modern alluvium used to estimate inheritance, CR-04 is considered less accurate because it probably contained contamination from material eroded from the nearby CR-03 sample site. The other modern alluvium sample, CR-06-01, was collected from higher up in the channel where it

could not have been contaminated by erosion of terrace material. However, a weighted mean inheritance was calculated using both CR-04 and CR-06-01 in order to not disregard any data that may influence the age of the *Qtf* fan. Fan surfaces southwest of the Camp Rock fault exist only as thin deposits; therefore it was impossible to obtain shielded samples from below the surface to further assess inheritance (Anderson et al., 1996). In addition, the thin surface deposit makes it difficult to independently gauge erosion of the fan surface. In many places *Qtf* gravels form a lag deposit upon eroding silt deposits.

To further constrain the age of *Qtf*, its morphology was compared with other dated alluvial fan surfaces formed in a similar environment. The properties of these alluvial fan surfaces have similar relative-age parameters to *Qtf* such as well-interlocked, smooth desert pavement with a dark varnish covering a majority of the clasts, rubified clast undersides, and extensive fan surfaces with no remaining original depositional morphology (i.e. bar and swale topography).

Based on a study by Dorn (1988) on Death Valley alluvial fans, *Qtf* surfaces along the Camp Rock fault can be correlated to his *Q3a* surfaces. Dorn (1988) described *Q3a* as having smooth and well-varnished desert pavements that are continuous over large areas. Older fans are highly dissected and have patchier desert pavement; younger fans have not developed enough desert pavement (Dorn, 1988). Nishiizumi et al. (1993) sampled clasts from the surfaces of these same Death Valley fans and dated those clasts using ^{10}Be and ^{26}Al cosmogenic radionuclides. The Hanaupah Canyon fan in Death Valley was selected for dating and yields a minimum apparent exposure age of 117±4 ka

(Nishiizumi et al., 1993). It is important to note that Nishiizumi does not consider inheritance in this study.

Studies by Bull (1991) on piedmonts from the lower Colorado River including the Whipple Mountains of southeastern California have *Q2c* and *Q2b* surfaces that are morphologically similar to *Qtf*. Based on one [^{230}Th/^{234}U] age obtained from clasts sampled from the surface, *Q2c* yields an age of 61 ka and seven clasts sampled from the *Q2b* surface yield an age of 82-83 ka (Bull, 1991)

Wells et al. (1987) and Reneau (1993) described surfaces from the Soda Mountains piedmont in the Mojave Desert. *Qf1* surfaces from these studies possess the same characteristics as *Qtf*. Although the *Qf1* surfaces have not been dated, Wells et al. (1995) collected and dated samples from a younger *Qf3* surface from the nearby Cima Dome area using cosmogenic ^{3}He. This fan produced ages of 85±9 ka and 80±10 ka from two aliquots of the same sample (Wells et al., 1995). From this age it can be deduced that *Qf1* surfaces are at least ~100 ka.

A recent study on the Lenwood fault, just west of the Camp Rock fault, includes relative and cosmogenic dating of alluvial fan surfaces adjacent to that fault. A *Qtf* surface along the Lenwood fault was sampled for clasts both at the surface and from a pit dug into the surface. Dating of these clasts using ^{10}Be cosmogenic radionuclides yielded an age of 200±30 ka (Strane, 2007). The Lenwood *Qtf* surface appears to possess the same geomorphic characteristics as the Camp Rock *Qtf* surface; however, its advanced age indicates the possibility that it is actually from an older fan generation.

The ages of 108±15 ka, 103±11, 71±9 and 78±14 ka determined from this study fall within the range of ages determined from other studies. Due to variable erosion on

the fan surface, the older ages of sample CR-01 are considered to be the most representative. By using these ages in conjunction with ages from other studies, a conservative age of 100±30 ka is assigned to the *Qtf* surface.

Slip Rate of the Camp Rock Fault

Slip rates are determined from alluvial fans that are dextrally displaced by the Camp Rock fault. Two well-defined offsets were located in the study area, one each in *Qtk* and *Qtf* fans. A maximum value and a minimum value of the offset *Qtf* fan were calculated by reconstructing the configuration of the fan and channel edges prior to disruption by faulting (Figure 8). The maximum offset of 66 m is based on matching the northwestern intersection of a *Qtf* terrace remnant with the fault with the contact of colluvium and basement rock on the opposite side of the fault. Any further backslipping of the fault results in the impossible placement of all or a portion of the *Qtf* alluvial fan remnant northeast of the fault behind a hill of basement rock southwest of the fault. The minimum offset is 16 m (Figure 8). This value is based on matching corresponding channel edges projected to the fault. The location of the usable northwest edge is estimated from existing topography. The minimum value of 16 m accounts for the fact that it is unknown if the original path of the channel was straight downhill at the time of abandonment of the fan surface, or if the channel had a distinct right deflection around the conglomerate hill west of the fault while it was depositing the terrace material. Dividing a *Qtf* offset of 41±25 m by a surface age of 100±30 ka yields a slip rate of 0.4±0.3 mm/yr for the Camp Rock fault.

An additional slip rate constraint is determined from minimum offset of the younger *Qtk* fan. This offset is formed as the fault displaced the edge of the *Qtk* fan and

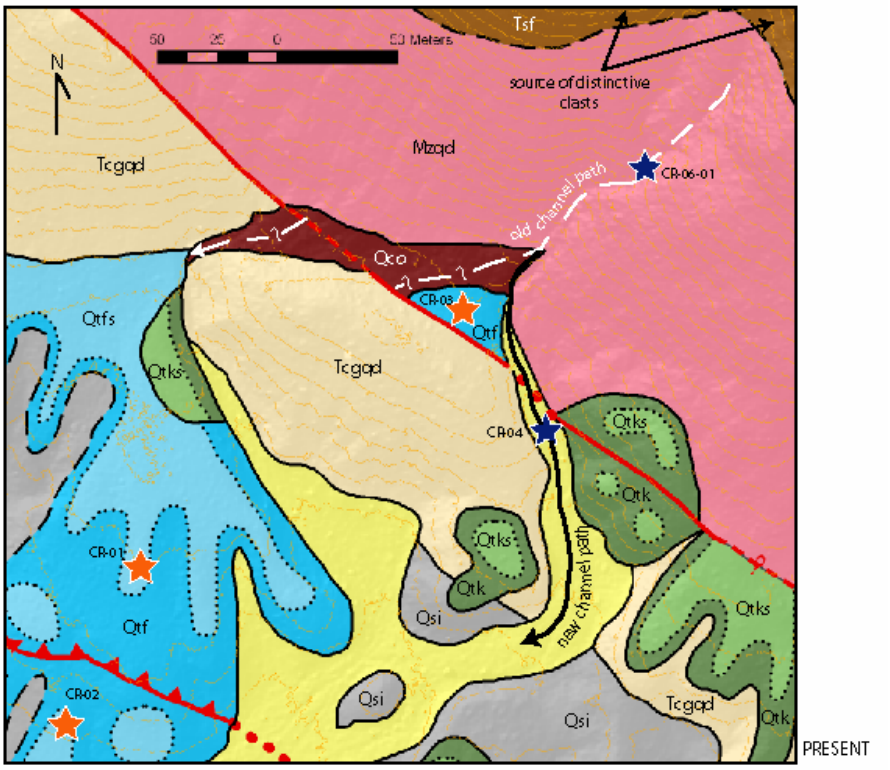
50 25 0 50 Meters
N
Tsf
source of distinctive clasts
Mzqd
Tcgqd
CR-06-01
old channel path
Qco
CR-03
Qtf
Qtfs
Qtks
Tcgqd
CR04
Qtks
Qtk
Qtks
Qtk
new channel path
CR-01
Qtf
Qsi
Qtks
CR02
Qsi
Qsi
Tcgqd
Qtk
PRESENT

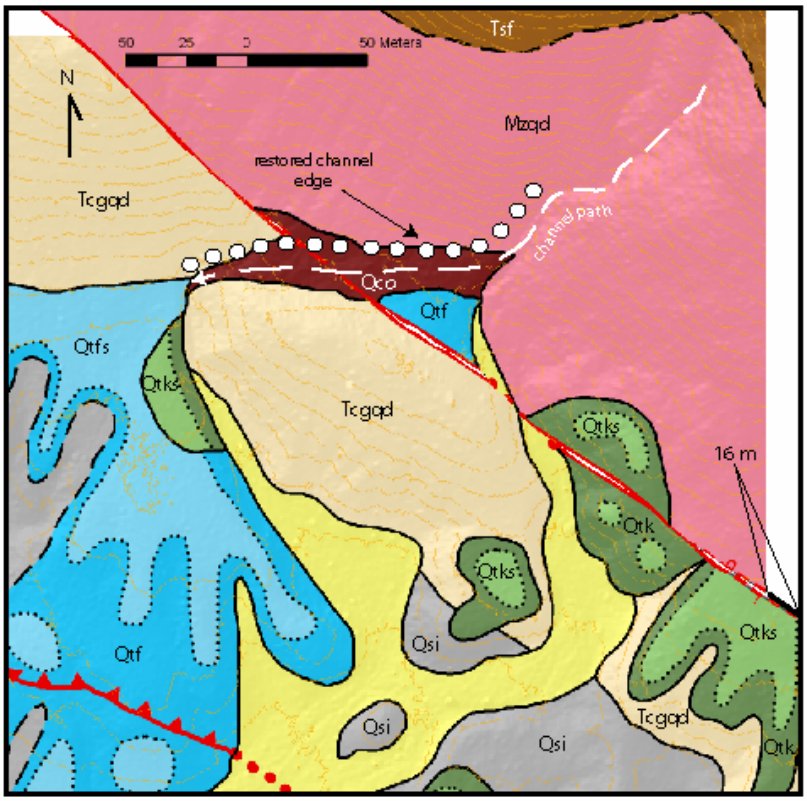
50 25 0 50 Meters
N
Tsf
Mzqd
restored channel edge
Tcgqd
channel path
Qco
Qtf
Qtfs
Qtks
Tcgqd
Qtks
16 m
Qtk
Qtks
Qtks
Qsi
Qtf
Qsi
Qsi
Tcgqd
Qtk
MINIMUM RESTORATION: 16 m

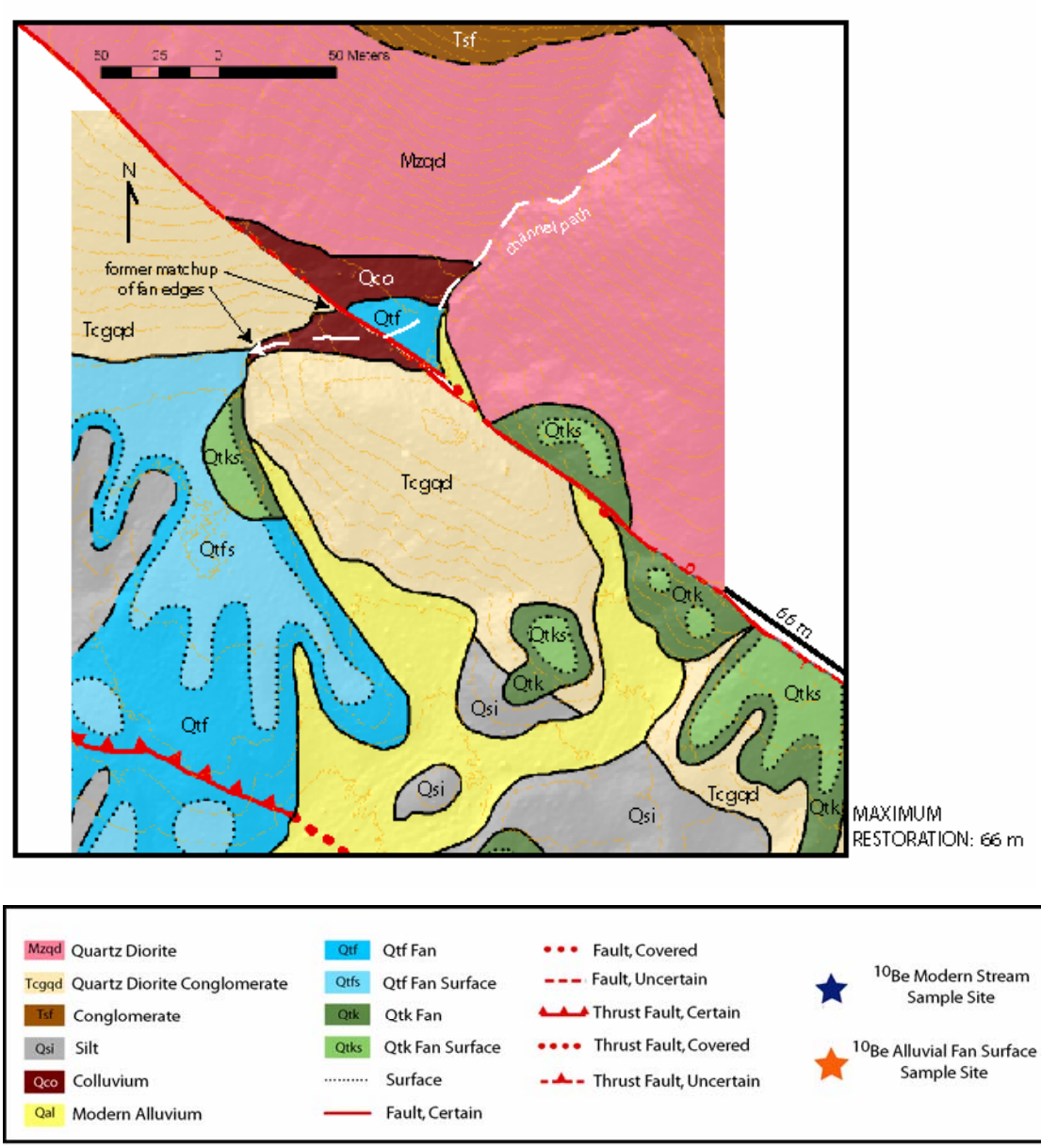

Figure 8: Restoration of slip along Camp Rock fault since truncation of Qtf alluvial fan. This Qtf fan is composed of mixed clasts, whereas other terraces in the area are composed only of quartz diorite. The distinctive clast makeup ensures that both the main portion of the Qtf fan and the truncated remnant were once part of a continuous fan. Former channel paths shown as white dashed lines; present day channel path as a solid black line. Top figure shows modern-day location of fan and remnant, along with the former and present channel paths. ^{10}Be sample sites are represented by stars. Middle figure shows 16 m minimum displacement, based on an inferred location of the restored northwest channel edge, represented by the line of white dots. Bottom figure shows 66 m maximum displacement, as any further displacement would impossibly situate the fan remnant on the northeast side of the fault behind a hill composed of quartz diorite conglomerate.

an inset alluvial fan channel by at least 22±2 m (Figure 9). This is a minimum offset because erosion could have occurred on the edge of the *Qtk* fan on the north side of the fault. Based on the work of Oskin et al. (2007), a *Qtk* alluvial fan surface along the nearby Calico fault (Figure 2) yielded a cosmogenic age of 56.4±7.7 ka. If this *Qtk* age is applied to the offset *Qtk* alluvial fan, a minimum slip rate of 0.4±0.1 mm/yr is obtained.

Folding of Lenwood Anticline

The Lenwood anticline is located at the northern tip of the Camp Rock fault. The axis of the fold trends approximately east-west. The south limb of the fold is comprised of Tertiary and Quaternary units that dip shallowly to the south or are flat-lying. Tertiary units consist of undifferentiated volcanic rocks and coarse conglomerates (*Tcv*), a mixed-clast conglomerate (*Tsf*), a granitic conglomerate (*Tsg*), sandstone and shale (*Tss*) and the Peach Springs Tuff (*Tpst*). At the core of the fold, which rises to an elevation of approximately 1300 m, Mesozoic granitic basement rocks are exposed. The north limb of the fold comprises Tertiary and Quaternary units. Older units dip more steeply than younger units. The undifferentiated volcanic rocks and coarse conglomerates (*Tcv*) found on the south limb are not exposed on the north limb. Tertiary units on the north limb consist of a granitic conglomerate (*Tsg*), sandstone (*Tss*), and the Peach Springs Tuff (*Tpst*; figure 4).

Based on the asymmetry of bedding dips, I interpret the Lenwood anticline as a fault-propagation fold. Beds in the steep limbs of fault-propagation folds progressively rotate toward the orientation of the fault with depth and proximity to fault (Erslev, 1991). In a limb rotation model, the younger beds syntectonically emplaced across the fold limb

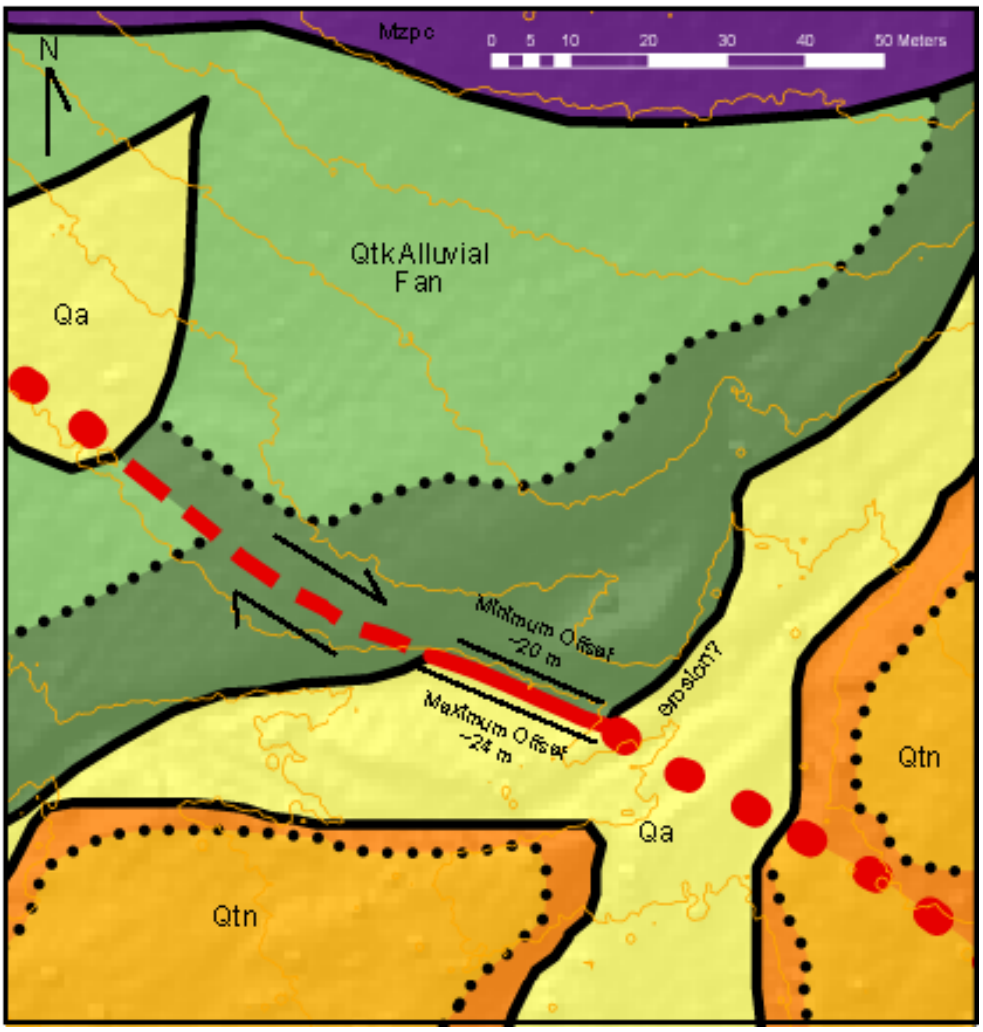

Figure 9. Offset of the Qtk age fan. The edge has been offset into a channel of modern alluvium. Offset is 22±2 m, which is measured as the edge of the Qtk fan is offset into a channel of modern alluvium. This offset is a minimum due to possible erosion of the Qtk fan northeast of the fault. Qtk = Quaternary tk fan, Qtn = Quaternary tn fan, Qa = modern alluvium, Mzpc = Mesozoic porphyry complex.

will dip less than older beds (Suppe et al., 1997). Dips measured on the north limb of the Lenwood anticline demonstrate limb rotation.

The Lenwood anticline has been an active fold since the Miocene. Active folding is exhibited by growth strata present on the north limb of the fold. These growth strata are characterized by internal unconformities that separate progressively younger beds on the north limb that dip more shallowly than the older beds. Uplifted and tilted terraces of *Qoa* are evidence of continued fold activity in the Quaternary.

DISCUSSION

To evaluate the constancy of slip rate over different time scales, slip rates for the Camp Rock fault obtained from offset alluvial fans are compared to paleoseismic slip rates and geodetic strain accumulation rates. By comparing these rates it becomes apparent that shorter-term paleoseismic slip rates are representative of long- and intermediate-term slip rates presented in this thesis. However, all of these geologic rates are low when compared to geodesy. Folding of the Lenwood anticline is then examined to determine whether contractional structures in the Mojave Desert accommodate as much deformation as faulting. Such folding may provide a mechanism by which discrepant geologic and geodetic strain rates can be reconciled.

Slip Rate Comparison

There are three basic time frames in which fault slip can be studied. Geodesy measures short-term present-day strain rates which can be used to establish corresponding displacement rates. However geodesy gives only a snapshot of a fault's loading rate during a small portion of the earthquake cycle. Paleoseismic trenching studies give earthquake recurrence rates that can be used to infer slip rates. Depending on the recurrence interval of earthquakes on a given fault, slip rates determined from paleoseismic investigations could encompass less than an entire earthquake cycle to one or two earthquakes. Slip rates measured in the long- to intermediate-term, such as those presented in this thesis, encompass slip accrued over many earthquakes and tens of

thousands of years. Examining these rates can encompass many complete earthquake cycles, thereby averaging shorter-term variations in slip rate and loading rate.

Paleoseismicity vs. long-term rate

For the Camp Rock fault, the average slip rate of 0.2-0.7 mm/yr determined from paleoseismic recurrence (Rubin and Sieh, 1997) is comparable to long-term slip rate of 0.4±0.3 mm/yr determined from this study. The *Qtk* minimum slip rate of 0.4±0.1 mm/yr, although less well-constrained, also falls within the range of paleoseismic estimates. Combining all of these constraints yields a best-estimate slip rate of 0.4 +0.3/-0.1 mm/yr for the Camp Rock fault.

Geologic vs. Geodetic Rate Reconciliation

The long-term slip rate of 0.4 +0.3/-0.1 mm/yr on the Camp Rock fault is 2%-7% of the present-day geodetic strain rate of 10-14 mm/yr across the central Mojave Desert. Because there are six dextral faults in this portion of the ECSZ, the total geodetic strain accumulation cannot be distributed evenly between these faults, as the Camp Rock fault does not account for 1/6 of the geodetic strain rate. Comparable pre- and post-Landers earthquake geodetic measurements suggest that this discrepancy is not due to post-seismic effects. One way the discrepancy can be reconciled is if there are faster faults in the ECSZ that account for more than 1/6 of the geodetic strain. For example, the slip rate on the Calico fault is 1.6±0.1 mm/yr (Oskin et al., 2007), or 11%-17% of the geodetic strain rate. However slip rates faster than that of the Calico fault are necessary on other faults to reconcile the discrepancy in strain rate across the entire shear zone. The contractional folds associated with some dextral faults of the ECSZ, including the Camp Rock fault, could also account for a portion of the rate discrepancy.

Role of Active Folding

There are two current viewpoints on the role of active folding in the central Mojave Desert. Dokka and Travis (1990) hypothesize that areas of shortening are local, minor components of total strain accumulation in the ECSZ. Bartley et al. (1990) state that north-south contraction is regionally significant in the central Mojave Desert. I modeled shortening of the Lenwood anticline in order to evaluate the importance of active folding in the area and relate it to slip on the Camp Rock fault.

Model of Lenwood anticline

A model of folding of the Lenwood anticline accounts for the following observations: (1) forelimb dips measured in the field and taken from mapping by Dibblee (1970), (2) evident but poorly constrained thickening of beds in the forelimb, (3) the location and dip of the backlimb, (4) lack of evidence for thrust-faulting at the surface, and (5) probable removal of *Tcv* on the forelimb by erosion (Figure 4 & Plate 2). The dip change within *Tsg* and the location and dips of the backlimb are the factors that provided the most important constraints on creating the fold model. Removal of *Tcv* is presumed to have occurred due to tilting and erosion during early Miocene extension prior to the onset of folding. If instead *Tcv* was eroded during uplift of the fold crest, additional shortening would be required.

I modeled the Lenwood anticline as a trishear fold using the FaultFold 4.6.4 modeling program of Allmendinger (1998; Figure 10). The three main variables considered in my model were fault angle, trishear angle, and P/S ratio. The trishear angle refers to the apical angle of the triangular zone in which deformation occurs ahead of a propagating fault. If the trishear angle is small, the deformation will be concentrated

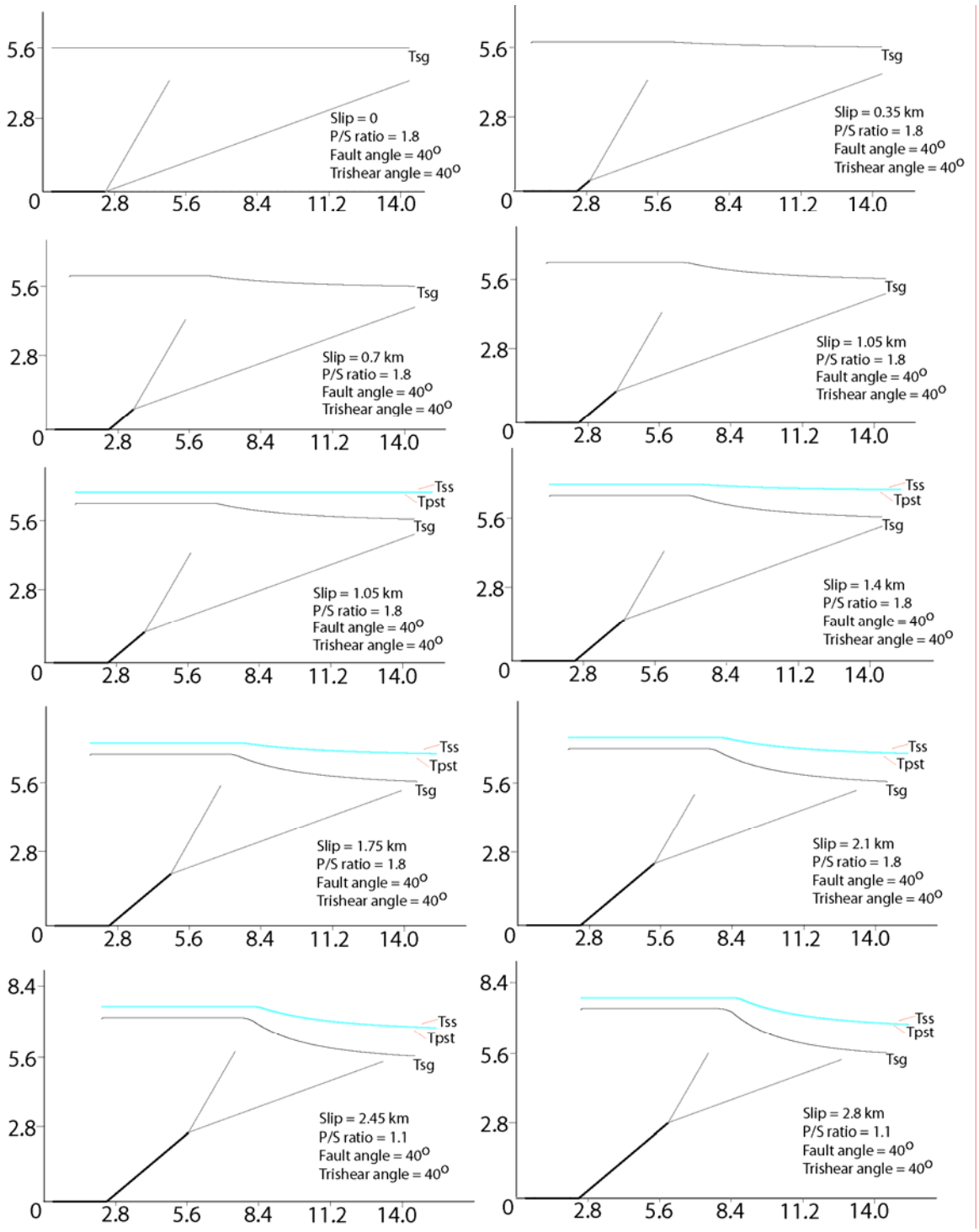
5.6
2.8
0
2.8
5.6
8.4
11.2
14.0
Tsg
Slip = 0
P/S ratio = 1.8
Fault angle = 40°
Trishear angle = 40°
Slip = 0.35 km
P/S ratio = 1.8
Fault angle = 40°
Trishear angle = 40°
Slip = 0.7 km
P/S ratio = 1.8
Fault angle = 40°
Trishear angle = 40°
Slip = 1.05 km
P/S ratio = 1.8
Fault angle = 40°
Trishear angle = 40°
Tss
Tpst
Slip = 1.05 km
P/S ratio = 1.8
Fault angle = 40°
Trishear angle = 40°
Slip = 1.4 km
P/S ratio = 1.8
Fault angle = 40°
Trishear angle = 40°
Slip = 1.75 km
P/S ratio = 1.8
Fault angle = 40°
Trishear angle = 40°
Slip = 2.1 km
P/S ratio = 1.8
Fault angle = 40°
Trishear angle = 40°
8.4
Slip = 2.45 km
P/S ratio = 1.1
Fault angle = 40°
Trishear angle = 40°
Slip = 2.8 km
P/S ratio = 1.1
Fault angle = 40°
Trishear angle = 40°

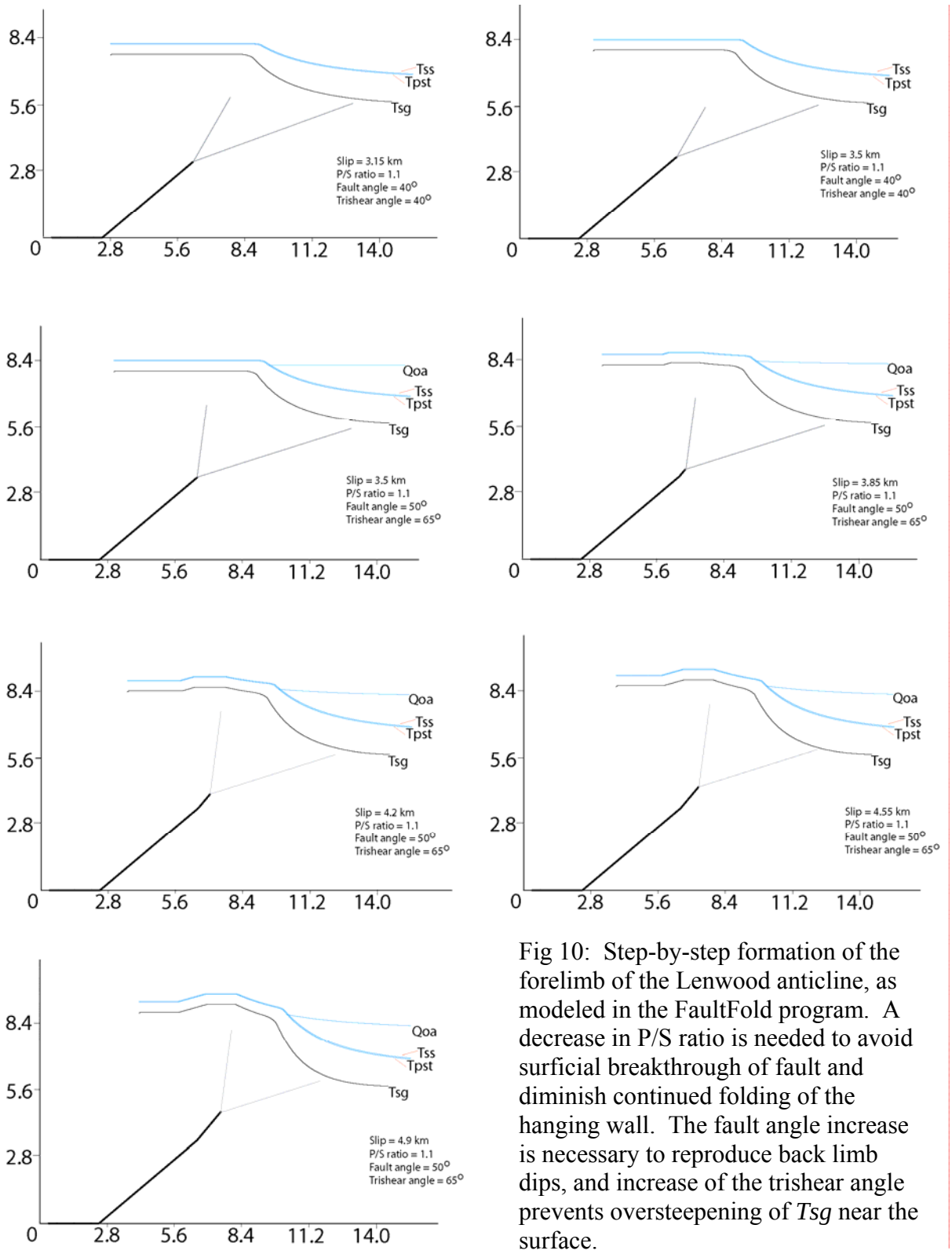

Fig 10: Step-by-step formation of the forelimb of the Lenwood anticline, as modeled in the FaultFold program. A decrease in P/S ratio is needed to avoid surficial breakthrough of fault and diminish continued folding of the hanging wall. The fault angle increase is necessary to reproduce back limb dips, and increase of the trishear angle prevents oversteepening of *Tsg* near the surface.

in a small wedge of rock, and if it is large, resulting deformation will be more diffuse (Allmendinger, 1998). The P/S ratio, or propagation to slip ratio, determines how quickly the fault tip propagates in relation to slip on the fault. For a large P/S ratio, material spends less time in the deformation zone, and is thereby less deformed. For a small P/S ratio, material will spend longer in the deformation zone and be more deformed. A P/S =1 indicates a trishear zone attached to the hanging wall (Allmendinger, 1998).

In order to reproduce the fold, I began the model with a fault dip of 40° and a trishear angle beginning at 40°. These initial values for fault angle and trishear angle were based on numerous trials of various fault and trishear angle combinations. Other combinations failed in that they either created folding that was too broad or tight, or did not concentrate folding in such a way as to produce the abrupt steepening of dip 19º to 67º in the forelimb.

The P/S ratio of 1.8 used through the first six folding steps helps to initiate the production of the dip change from 19º to 67º in *Tsg*. A higher P/S ratio results in fault tip placement too close to the beds, thereby producing drastic oversteepening in the shallowly dipping portion of *Tsg* and the other beds. Four more folding steps occur with the P/S ratio decreasing to 1.1. This decrease is needed to avoid breakthrough of the fault at the surface and diminish folding in upper layers of the hanging wall such as *Tss* and *Qoa*. Even lower P/S ratios were unable to create the 19º dip in *Tsg*.

To produce the change from 0º to 15º in the backlimb, the fault angle was changed to 50º and the trishear angle increases to 65º during the final four steps of folding, while the P/S ratio was maintained at 1.1. This fault angle change can reproduce

the dips in the back limb (Narr and Suppe, 1994) and also sets it the appropriate distance away from the forelimb. Folding of the backlimb was iteratively determined from the fold model using angular relationships set forth by Narr and Suppe (1994),

$$\theta = \tan^{-1}[1/(\cot\phi - \cot(\beta + \phi) + \cot(\phi + \varepsilon))] - \phi,$$

where θ is the lower fault dip, ϕ is the dip of the axial plane of the backlimb fold, β is the backlimb dip, and ε is the upper fault dip.

All angles used to model the cross-section in FaultFold 4.6.4 are within 2º of those determined from the equation of Narr and Suppe (1994). Once the fault dip had been steepened, it became essential to widen the trishear angle. In previous models where the trishear angle was not widened, the steeper fault angle caused too much steepening in *Tsg* near the surface, and resulted in excess folding to be located where it was not needed. Widening of the trishear angle smoothes out this oversteepening and maintains the proper location of continued folding.

Shortening and its Relationship to Slip on the Camp Rock fault

The value of shortening across the Lenwood anticline is estimated to be 3.8 km (Figure 11A). This value is determined from the modeled amount of fault slip (4.9 km) and the dip of the lower portion of the fault (40°). This estimate is of the same order as the 2 to 4 km of slip determined from basement rocks offset across the Camp Rock fault (Hawkins, 1976; Miller, 1980; Figure 3). However, because the Camp Rock fault strikes NW and the fold axis strikes EW, an additional geometric correction is needed to compare dextral fault slip to shortening. If the 3.8 km of shortening represents only the NS component of the slip vector on the Camp Rock fault (Figure 11B), the length of this

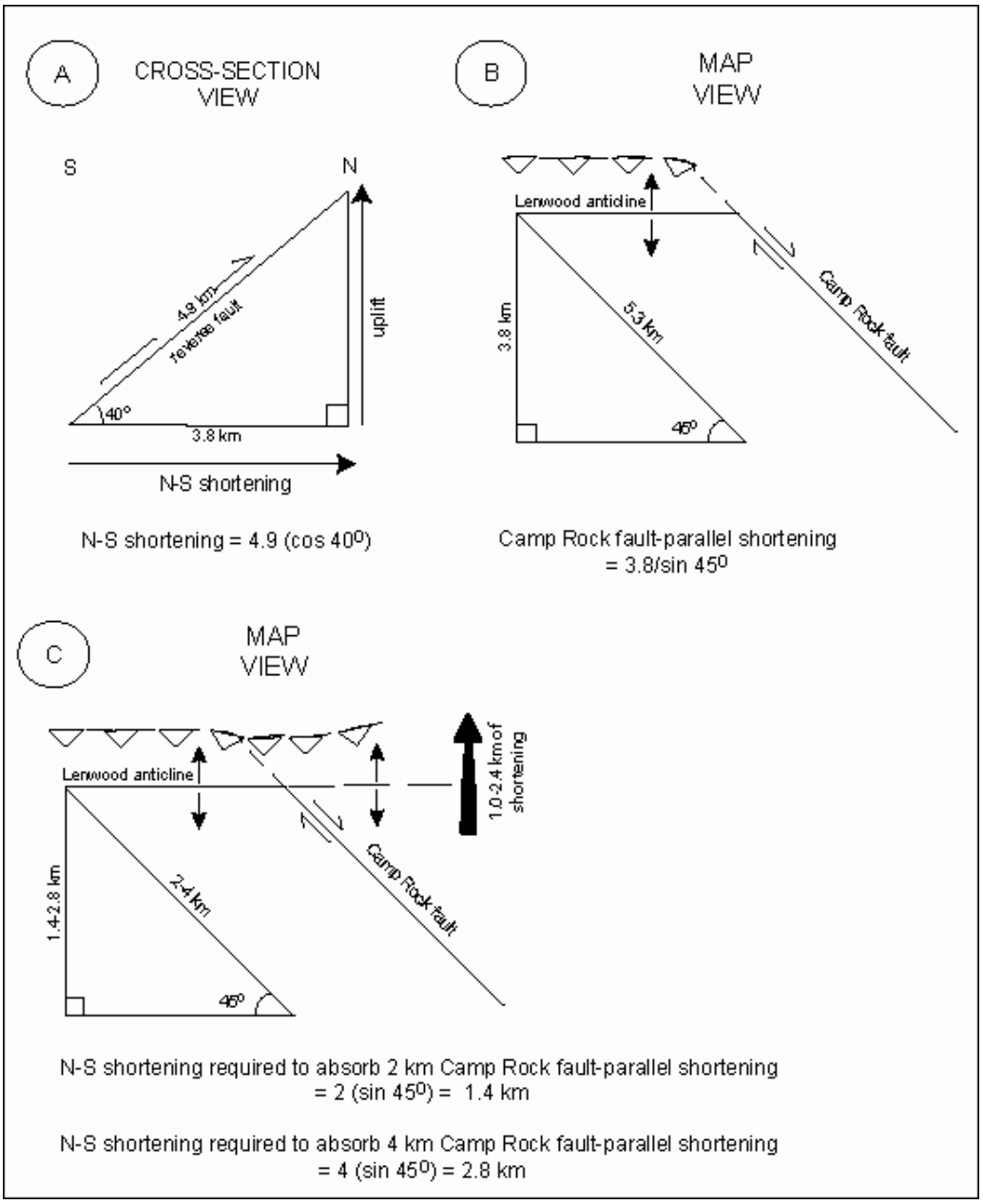

Figure 11. Cross-section view and map view of slip on the Camp Rock fault and shortening on the Lenwood anticline. Trigonometric relationships were used to determine shortening values from existing data. (A) shows N-S shortening across the anticline, 3.8 km. 4.9 km slip on the reverse fault is data obtained from modeling of the fold. (B) shows shortening of the Lenwood anticline parallel to the Camp Rock fault, 5.3 km. (C) shows the amount of N-S shortening needed to yield values that absorb total slip on the Camp Rock fault with no excess, 1.4-2.8 km. Extension of thrust fault on the right-hand side of the Camp Rock fault in (C) is suggested by Glazner and Bartley (1994).

vector would be

$$3.8 \text{ km} / \sin 45^\circ = 5.3 \text{ km}$$

This is at least ~1 km greater than the amount of slip recognized on the Camp Rock fault.

Understanding that the Lenwood anticline has experienced enough shortening to absorb all Camp Rock fault slip has important implications for how strain is accommodated within the Mojave Desert portion of the ECSZ. It is not necessary to look for or assume throughgoing faults to the north and south of Barstow, such as those presented in the Mojave Block deformation model of Garfunkel (1974). The significance of folding in the central Mojave Desert appears to be congruent with the hypotheses of Bartley et al. (1990) and Glazner et al., (2002) that north-south shortening is an important component of strain accumulation that could help to reconcile the discrepancy between geologic and geodetic strain measurements. The important observation is that there is more shortening on the Lenwood anticline than can be accommodated by Camp Rock fault slip. This indicates that north-south shortening may partially reconcile the geologic slip rate and geodetic strain rate discrepancy regionally across the central Mojave Desert.

Figure 11C shows a map-view model where some shortening on the Lenwood anticline is not transferred to slip on the Camp Rock fault. Rather, this shortening continues on an eastward extension of the Lenwood anticline beneath the Newberry Mountains. Such a continuation of the thrust fault that underlies the Lenwood anticline has previously been hypothesized (Bartley et al., 1990, 1992; Glazner and Bartley, 1994). Of the 3.8 km of north-south shortening west of the Camp Rock fault, 1.0 to 2.4 km is maintained east of the Camp Rock fault. This shortening contributes to regional north-south contraction of the Mojave Block that could accommodate some of the Pacific-North America plate motion not absorbed by dextral faulting (Bartley et al. 1990).

Presently the rates of such shortening are not well known, so it is difficult to further evaluate its role in reconciling the geologic-geodetic rate discrepancy.

CONCLUSIONS

Based on offsets located through detailed mapping along the Camp Rock fault and assigning ages to these surfaces based on ^{10}Be dating and correlation with previous work (Bull, 1991; Dorn, 1988; Wells et al., 1987; Nishiizumi et al., 1993; Reneau, 1993; Wells et al., 1995; Oskin et al., 2007, Strane, 2007), the slip rate on the Camp Rock fault is 0.4 +0.3/-0.1 mm/yr. This slip rate agrees with the 0.2-0.7 mm/yr rate determined from paleoseismic studies of the Emerson fault, an along-strike continuation of the Camp Rock fault (Rubin and Sieh, 1997). The comparable paleoseismic and long-term slip rates confirm that Holocene activity on the fault is representative of activity over the past 100 kyr. The Camp Rock fault contributes only 2-7% of geodetically measured strain accumulation across the Mojave Desert portion of the ECSZ.

Contractional structures associated with various strike-slip faults in the central Mojave Desert, (i.e. the Lenwood anticline) are capable of accommodating as much strain as dextral faulting. Based on evidence of limb rotation on the Lenwood anticline, a trishear fault-propagation fold was used to model shortening. The shortening amount of 3.8 km is comparable to total slip on the Camp Rock fault of 2 to 4 km (Hawkins, 1976; Miller, 1980). Because this north-south shortening is oblique to the northwest strike of the Camp Rock fault, there is potential that shortening exceeds the amount needed to absorb all Camp Rock fault slip. Based on the map-view relationship of folding to faulting, up to 1.0 to 2.4 km of shortening of the Lenwood anticline may contribute to

regional contraction of the Mojave Block. Though the rate of this regional contraction has not yet been determined, it likely contributes towards reconciling discrepant geologic and geodetic rates across the Mojave ECSZ.

APPENDIX A: Cosmogenic ^{10}Be Sample Preparation

Samples were first described based on clast composition, and then crushed and sieved to 0.2 – 0.25 mm. This fraction was then leached in heated 6N hydrochloric acid to remove any carbonates, iron oxides or minor organic matter present on the samples. The remaining sample was then leached in 1% hydrofluoric acid (HF) and 1% nitric acid (HNO_3) in a sonic bath to etch the quartz grains to remove meteoric ^{10}Be, and to remove residual feldspar and clay minerals. This step was at least thrice repeated, with the amount of sample loss noted in between each leaching. The majority of sample loss occurred during the first step.

The samples were then precisely weighed, divided into vials, and spiked with 0.3 grams of ^{9}Be (SPEX standard), to ensure accurate measurements of the ^{9}Be/^{10}Be ratio using the accelerator mass spectrometer. The spiked samples were then dissolved in a 3:1 HF/ HNO_3 solution and heated on hot plates to fume away SiO_2. Remaining fluorine ions were fumed away using perchloric acid.

The samples were run through both anion and cation columns to remove every remaining impurity in the sample other than Be. To precipitate out the Be gel from the ambient fluid, a Be and 6N HCl solution was neutralized with 8N ammonium hydroxide, and the samples were placed into a centrifuge. Oven-drying of the samples in a hot block was followed by oxidization in a furnace at 750 °C. This turned the Be gel into dust which was then mixed with niobium powder and packed into targets.

REFERENCES

Allmendinger, R.W., 1998, Inverse and forward numerical modeling of trishear fault-propagation folds: Tectonics, v. 17, no. 4, p. 640-656.

Anderson, R.S., Repka, J.L., and Dick, G.S., 1996, Explicit treatment of inheritance in dating depositional surfaces using in situ (super 10) Be and (super 26) Al: Geology, v. 24, n. 1, p. 47-51.

Atwater, T., 1970, Implications of plate tectonics for the Cenozoic tectonic evolution of western North America: Geological Society of America Bulletin, v. 81, n. 12, p. 3513-3535.

Bartley, J.M., Glazner, A.F., and Schermer, E.R., 1990, North-south contraction of the Mojave block and strike-slip tectonics in southern California: Science, v. 248, p. 1398-1401.

Bartley, J.M., Glazner, A.F., Fletcher, J.M., Martin, M.W., and Walker, J.D., 1992, Amount and nature of dextral offset on Neogene faults near Barstow, California, *in* Eos, Transactions of the 1992 Fall Meeting of the American Geophysical Union: San Francisco, CA, American Geophysical Union, p. 363.

Bull, W.B., 1991, Geomorphic Responses to Climate Change: New York, Oxford University Press, 326 p.

Carter, J.N., Luyendyk, B.P., and Terres, R.R., 1987, Neogene clockwise tectonic rotation of the eastern Transverse Ranges, California, suggested by paleomagnetic vectors: Geological Society of America Bulletin, v. 98, p. 199-206.

Crowell, J.C., 1981, An outline of the tectonic history of southeastern California, *in* Ernst, W.G., ed., The geotectonic development of California (Rubey vol. 1): Englewood Cliffs, New Jersey, Prentice-Hall, p. 583-600.

Dawson, T., McGill, S.F., and Rockwell, T.K., 2003, Irregular recurrence of paleoearthquakes along the central Garlock fault near El Paso Peaks, California: Journal of Geophysical Research, v. 108, no. B7, p. DOI: 10.1029/2001JB001744.

Dibblee, T.W., 1961, Evidence of strike-slip movement on northwest-trending faults in Mojave Desert, California: U.S. Geological Survey Professional Paper, v. 424-B, p. 197-198.

Dibblee, T.W., 1964, Geological Map of the Ord Mountains Quadrangle, San Bernardino County, California, Miscellaneous Geologic Investigations Map I-427: Washington D.C., U.S. Geological Survey.

Dibblee, T.W., 1964, Geological Map of the Rodman Mountains Quadrangle, San Bernardino County, California, Miscellaneous Geologic Investigations Map I-430: Washington D.C., U.S. Geological Survey.

Dibblee, T.W., 1970, Geological Map of the Daggett Quadrangle, San Bernardino County, California, Miscellaneous Geologic Investigations Map I-592: Washington D.C., U.S. Geological Survey.

DeMets, C., and Dixon, T.H., 1999, New kinematic models for Pacific-North America motion from 3 Ma-present, I: Evidence for steady motion and biases in the NUVEL-1A model: Geophysical Research Letters, v. 31, n. 7, p. 1921-1924.

Dixon, T.H., Robaudo, S., Lee, J., and Reheis, M.C., 1995, Constraints on present-day Basin and Range deformation from space geodesy: Tectonics, v. 14, p. 755-772.

Dokka, R.K., 1983, Displacements on late Cenozoic strike-slip faults of the central Mojave Desert, California: Geology, v. 11, p. 305-308.

Dokka, R.K., 1989, The Mojave extensional belt of southern California: Tectonics, v. 8, p. 363-390.

Dokka, R.K., and Travis, C.J., 1990, Late Cenozoic strike-slip faulting in the Mojave Desert, California: Tectonics, v. 9, p. 311-340.

Dorn, R.I., 1988, A Rock Varnish Interpretation of Alluvial-fan Development in Death Valley, California: National Geographic Research, v. 4, no. 1, p. 56-73.

Erslev, Eric, 1991, Trishear fault-propagation folding: Geology, v. 19, p. 617-620.

Fletcher, J.M., Bartley, J.M., Martin, M.W., Glazner, A.F., and Walker, J.D., 1995, Large-magnitude continental extension; an example from the central Mojave metamorphic core complex: Geological Society of America Bulletin, v. 107, no. 12, p. 1468-1483.

Gan, W., Svarc, J.L., Savage, J.C., and Prescott, W.H., 2000, Strain accumulation across the Eastern California Shear Zone at latitude 36°30'N: Journal of Geophysical Research, v. 105, p. 16229-16236.

Garfunkel, Z., 1974, Model for the Late Cenozoic Tectonic History of the Mojave Desert, California, and for Its Relation to Adjacent Regions: GSA Bulletin, v. 85, p. 1931-1944.

Glazner, A.F., and Bartley, J.M., 1994, Eruption of alkali basalts during crustal shortening in southern California: Tectonics, v. 13, no. 3, p. 493-498.

Glazner, A.F., Walker, D.J., Bartley, J.M., and Fletcher, J.M., 2002, Cenozoic evolution of the Mojave block of southern California: Geological Society of America Memoir, v. 195, p. 19-41.

Hawkins, H.G., 1976, Strike slip displacement along the Camp Rock fault, central Mojave Desert, San Bernardino, California [Masters Thesis]: University of Southern California, 63 p.

Hewett, D.F., 1954, A fault map of the Mojave Desert region, [Pt.] 2, Chap. 4 of Jahns, R.H., ed., Geology of southern California: California Division of Mines Bulletin, 170, p. 15-18.

Lal, D., 1991, Cosmic ray labeling of erosion surfaces: in-situ nuclide production rates and erosion models: Earth and Planetary Science Letters, v. 104, p. 429-439.

McQuarrie, N., and Wernicke, B.P., 2005, An animated tectonic reconstruction of southwestern North America since 36 Ma: Geosphere, v. 1, no. 3, p. 147-172.

Miller, M.M., Johnson, D. J., Dixon, T.H., and Dokka, R.K., 2001, Refined Kinematics of the Eastern California shear zone from GPS observations: Journal of Geophysical Research, v. 106, p. 2245-2264.

Miller, S.T., 1980, Geology and mammalian biostratigraphy of a part of the northern Cady Mountains, Mojave Desert, California: U.S. Geological Survey Open-File Report 80-878, 122 p.

Narr, W., and Suppe, J., 1994, Kinematics of Basement-Involved Compressive Structures: American Journal of Science, v. 294, p. 802-860.

Nishiizumi, K., Kohl, C.P., Arnold, J.R., Dorn, R., Klein, J., Fink, D., Middleton, R., Lal, D., 1993, Role of *In Situ* Cosmogenic Nuclides ^{10}Be and ^{26}Al in the Study of Diverse Geomorphic Processes: Earth Surface Processes and Landforms, v. 18, p. 407-425.

Oskin, M., and Iriondo, A., 2004, Large-magnitude transient strain accumulation on the Blackwater fault, Eastern California shear zone: Geology, v. 32, no. 4, p. 313-316.

Oskin, M., Perg, L., Blumentritt, D., Mukhopadhyay, S., Iriondo, A., 2007, Slip rate of the Calico fault: Implications for geologic versus geodetic rate discrepancy in the Eastern California shear zone, 31 pp.

Reneau, Steven L., 1993, Manganese accumulation in Rock Varnish on a Desert Piedmont, Mojave Desert, California, and Application to Evaluating Varnish Development: Quaternary Research, v. 40, p. 309-317.

Rockwell, T.K., Lindvall, S., Herzberg, M., Murbach, D., Dawson, T., and Berger, G., 2000, Paleoseismology of the Johnson Valley, Kickapoo, and Homestead Valley Faults: Clustering of Earthquakes in the Eastern California Shear Zone: Bulletin of the Seismological Society of America, v. 90, 5, p. 1200-1236.

Rubin, Charles M., and Sieh, Kerry, 1997, Long dormancy, low slip rate, and similar slip-per-event for the Emerson fault, eastern California shear zone: Journal of Geophysical Research, v. 102, no. B7, p. 15319-15333.

Sauber, J., Thatcher, W., Solomon, S.C., 1986, Geodetic Measurement of Deformation in the Central Mojave Desert, California: Journal of Geophysical Research, v. 91, no. B12, p. 12683-12693.

Sauber, J., Thatcher, W., Solomon, S.C., Lisowski, M., 1994, Geodetic slip rate for the eastern California shear zone and the recurrence time of Mojave desert earthquakes: Nature, v. 367, p. 264-266.

Savage, J.C., Lisowsky, M., and Prescott, W.H., 1990, An apparent shear zone trending north-northwest across the Mojave Desert into Owens Valley, eastern California: Geophysical Research Letters, v. 12, p. 2113-2116.

Sieh, K.E., Jahns, R.H., 1984, Holocene activity of the San Andreas Fault at Wallace Creek, California: Geological Society of America Bulletin, v. 95, n. 8, p. 883-896.

Sieh, K., Jones, L., Hauksson, E., Hudnut, K., Eberhart-Phillips, D., Heaton, T., Hough, S., Hutton, K., Kanamori, H., Lilje, A., Lindvall, S., McGill, S.F., Mori, J., Rubin, C., Spotila, J.A., Stock, J., Thio, H.K., Treiman, J., Wernicke, B., and Zachariassen, J., 1993, Near-Field Investigations of the Landers Earthquake Sequence, April to July, 1992: Science, v. 260, p. 171-176.

Stewart, J.H., 1983, Extensional tectonics in the Death Valley area, California, Transport of the Panamint Range structural block 80 km northwest: Geology, v. 11, p. 153-157.

Stone, J.O., 2000, Air pressure and cosmogenic isotope production: Journal of Geophysical Research, v. 105, p. 23753-23759.

Strane, M.D., 2007, Slip rate and structure of the nascent Lenwood fault zone, Eastern California [Masters Thesis]: The University of North Carolina at Chapel Hill, 65 p.

Suppe, J., Sábat, F., Muñoz, J.A., Poblet, J., Roca, E., and Vergés, J, 1997, Bed-by-bed fold growth by kink-band migration: Sant Llorenç de Morunys, eastern Pyrenees: Journal of Structural Geology, v. 19, nos. 3-4, p. 443-461.

Treiman, J.A., Kendrick, K.J., Bryant, W.A., Rockwell, T.K. and McGill, S.F., 2002, Primary Surface Rupture Associated with the M_W 7.1 16 October 1999 Hector Mine Earthquake, San Bernardino County, California: Bulletin of the Seismological Society of America, v. 92, no. 4, p. 1171-1191.

Wells, S.G., McFadden, L.D. and Dohrenwend, J.C., 1987, Influence of Late Quaternary Climatic Changes on Geomorphic and Pedogenic Processes on a Desert Piedmont, Eastern Mojave Desert, California: Quaternary Research, v. 27, p. 130-146.

Wells, S.G., McFadden, L.D., Poths, J., and Olinger, C.T., 1995, Cosmogenic ^{3}He surface-exposure dating of stone pavements: Implications for landscape evolution in deserts: Geology, v. 23, no. 7, p. 613-616.